Biogeosciences Discuss., 11, 4047–4083, 2014
www.biogeosciences-discuss.net/11/4047/2014/
doi:10.5194/bgd-11-4047-2014

Biogeosciences Discussions
Open Access

CO_2 and CH_4 in sea ice from a subarctic fjord

O. Crabeck[1], B. Delille[2], D. N. Thomas[3,4], N. X. Geilfus[6], S. Rysgaard[1,5,6], and J. L. Tison[7]

[1]Center for Earth Observation Science, Department of Geological Science, University of Manitoba, Winnipeg, MB, R3T 2N2, Canada
[2]Unité d'Océanographie Chimique, Université de Liège, Liège, 4000, Belgium
[3]School of Ocean Sciences, Bangor University, Menai Bridge, Anglesey LL59 5AB, UK
[4]Marine Research Centre, Finnish Environment Institute, Helsinki, Finland
[5]Greenland Climate Research Centre, c/o Greenland Institute of Natural Resources, 3900 Nuuk, Greenland
[6]Arctic Research Centre, Aarhus University, 8000 Aarhus, Denmark
[7]Laboratoire de Glaciologie, D.S.T.E., Université Libre de Bruxelles, Bruxelles, 1050, Belgium

Received: 29 January 2014 – Accepted: 15 February 2014 – Published: 12 March 2014

Correspondence to: O. Crabeck (crabecko@myumanitoba.ca)

Published by Copernicus Publications on behalf of the European Geosciences Union.

Abstract

We present CH_4 concentration [CH_4] and the partial pressure of CO_2 (pCO_2) in bulk sea ice from subarctic, land-fast sea ice in the Kapisillit fjord, Greenland. The bulk ice [CH_4] ranged from 1.8 to 12.1 nmol L^{-1}, which corresponds to a partial pressure range of 3 to 28 ppmv. This is markedly higher than the average atmospheric methane content of 1.9 ppmv. Most of the trapped methane within the sea ice was evidently contained inside bubbles, and only a minor portion was dissolved in the brine. The bulk ice pCO_2 ranged from 60 to 330 ppmv showing that sea ice at temperatures above −4 °C is under-saturated compared to the atmosphere (390 ppmv). Our study adds to the few existing studies of CH_4 and CO_2 in sea ice and concludes that sub-arctic sea can be a sink for atmospheric CO_2, while being a net source of CH_4. Processes related to the freezing and melting of sea ice represents large unknowns to the exchange of CO_2 but also CH_4. It is therefore imperative to assess the consequences of these unknowns through further field campaigns and targeted research under other sea ice conditions at both hemispheres.

1 Introduction

The main driver of climate warming is the accumulation of greenhouse gases such as CO_2, CH_4 and N_2O within the atmosphere. Among these, CO_2 is the most important in terms of radiative forcing followed by methane (Ramaswamy et al., 2001). The concentrations of these gases in the atmosphere are 390 ppmv and 1.9 ppmv, respectively (2013 levels - http://www.esrl.noaa.gov/gmd/aggi/). Sea ice was for long considered as an inert barrier for gas exchange between the atmosphere and the ocean (Tison et al., 2002), but there is growing evidence to suggest that sea ice might contribute to the exchanges of significant fluxes of climatically active biogases (CO_2, CH_4) between the ocean and the atmosphere (Delille et al., 2007; Geilfus et al., 2012a, 2013a; Nomura et al., 2010, 2013; Semiletov et al., 2004; Zemmelink et al., 2006). However, the re-

BGD
11, 4047–4083, 2014

gional and global-scale impacts of sea ice on such gas exchanges are still unknown (Parmentier et al., 2013).

While the Arctic Ocean acts as pump for the atmospheric CO_2 (Bates and Mathis, 2009; Takahashi et al., 2009), recent studies show that the Arctic Ocean is a net source of atmospheric methane (Parmentier et al., 2013). Indeed, recent airborne measurements in the central Arctic basin have shown substantial methane emissions around $2\,mg\,m^{-2}\,d^{-1}$ in area of open leads and fractional ice cover (Parmentier et al., 2013). Moreover, Damm et al. (2005, 2007, 2010) and Kort et al. (2012) reported methane super-saturation in Arctic surface waters and point to sediments as being the main sources. Several studies have suggested that methane accumulates in Arctic waters underlying sea ice, where it can subsequently be oxidised (Kitidis et al., 2010; Kvenvolden et al., 1993; Savvivech et al., 2003; Shakova et al., 2010). While methane oxidation is one of the known sinks for methane, the future retreat of the Arctic sea ice cover could limit the residence time of methane in the water column and in turn the rates of methane oxidation. Parmentier et al. (2013) report a positive correlation between sea ice cover extent and methane emissions confirming the relationship between reduced sea ice extent and potential impact on gas exchange around the Arctic Ocean. However, to our knowledge, few studies have focused directly on CH_4 within sea ice itself (Zhou et al., 2014). Sea ice is an effective barrier to turbulent diffusion and ebullition flux across the sea–air interface, but being one of the largest biomes, it is an interface for CH_4 storage and transformation through biogeochemical processes.

Climatological reconstructions of air–sea CO_2 fluxes show that the polar oceans act as significant atmospheric CO_2 sinks, although the complexity and coverage of sea ice are still poorly represented (Takahashi et al., 2009). Studies by Delille et al. (2007) and Geilfus et al. (2012a) provide evidence that during spring and summer, CO_2 concentrations in sea ice brines reach minimum levels due to the combined effects of brine dilution, calcium carbonate dissolution and algal photosynthesis. Hence, sea ice acts as a carbon pump during spring and summer. In contrast, during ice formation there are indications that sea ice acts as a CO_2 source as a consequence of the concentra-

BGD
11, 4047–4083, 2014

tion of solutes in brines, $CaCO_3$ precipitation and microbial respiration (Geilfus et al., 2013b; Nomura et al., 2006; Tison et al., 2008).

Overall, there are many uncertainties regarding CO_2 dynamics within Arctic sea ice partly due to poor data coverage and also because of the recent discoveries of several processes in the carbonate system which combine to influence the overall budget of air-ice CO_2 fluxes over sea ice (Dellile et al., 2007; Rysgaard et al., 2011, 2013). In this study, we had two main objectives: (1) to perform measurements of CH_4 concentrations in bulk sea ice, thereby gaining key information for assessing the potential effect of sea ice on the methane emission budget in ice covered seas. (2) To add further to the understanding of pCO_2 dynamics in sea ice. We carried out measurements of the spatial and temporal distributions of pCO_2 in surface ice. These are of primary importance in order to evaluate the role of Arctic sea ice in the carbon cycle (Parmentier et al., 2013). The survey took place in a subarctic frozen fjord (SW Greenland) in March 2010. Fjord systems contrast to shelf environments because they are often under the influence of a fresh water input. Our study, therefore, also provides the opportunity to document the interaction between the landfast sea ice and the riverine input.

2 Field work

2.1 Study site

Sampling was conducted from 10 March to 16 March 2010 on first-year land-fast sea ice in Kapisillit, in the vicinity of Nuuk, SW Greenland (64°26° N 50°13° W) (Fig. 1). The salinity of the seawater in the fjord was 32.9. During this study, the air temperatures ranged from −8.8 °C to +2.9 °C, with an average temperature of −3.2 °C. The water depth at the location was between 40 and 45 m. The survey took place before the onset of the algae bloom and the concentrations of chlorophyll *a*, documented in Søgaard et al. (2013) and in Long et al. (2012), were $2.8 \pm 0.4\,\mu g\,L^{-1}$ (SE, $n = 3$) in the bottom

BGD
11, 4047–4083, 2014




12 cm of ice, and the average concentration across the entire ice thickness was 1.0 ± 1.2 µg L^{-1} (SE, n = 3) (Long et al., 2012).

2.2 Field sampling

To follow the temporal evolution of the sea ice, we sampled four times in sea ice and water column at the same station at 4 different time periods; 11 March, 13 March, 15 March and 16 March. Sampling was achieved within an area of about 25 m^2 in order to minimize bias from spatial heterogeneity. For each station, 5 ice cores were extracted using a Kovacs drill corer with internal diameter of 9 cm (Kovacs Ent., Lebanon, USA). Cores were immediately wrapped in polyethylene bags and stored on the sampling site in an insulated box, with cooling bags (precooled at −20 °C) to ensure brine and gas immobilization and inhibit biological processes (Eicken et al., 1991). Back in the laboratory, the ice cores were stored in a cold room at −25 °C before further gas extraction and analyses.

Ice temperature was measured in situ, immediately after the ice core extraction, at a depth resolution of 5 cm. A calibrated probe (Testo 720, Hampshire, UK) was used by inserting it into pre-drilled holes perpendicular to the ice core axis with the same diameter of the probe. The precision of the probe was ±0.1 °C. This "temperature" ice core was immediately cut into 5 cm slices, which were then stored in individual polyethylene pots and left to melt at 4 °C. Bulk ice salinity was measured with a conductivity meter (Orion Star Series Meter WP-84TP, Beverly, USA) which had a precision of ±0.1 for deduced salinity.

Brines were sampled using the sackhole sampling technique at 20 cm and 40 cm below the ice surface (Gleitz et al., 1995). Each sackhole was covered with a plastic lid to avoid snow and ice shavings falling into the pit (Thomas et al., 2010). Under ice seawater samples were collected through the ice core hole, at 0, 1 and 9 m depth. Both brine and seawater were collected using a peristaltic pump (Cole Palmer, Masterflex® – Environmental Sampler). Samples for dissolved methane were stored in 60 mL vials poisoned with saturated mercury chloride ($HgCl_2$).

BGD
11, 4047–4083, 2014

3 Analysis

3.1 Ice texture

To describe the texture of the ice, horizontal thin sections were produced for each 10 cm section of the entire ice column, using the standard microtone (Leica SM2400) procedure described by Langway (1958) and Tison et al. (2008). The images from horizontal thin sections were recorded with a camera (Nikon Coolpix S200) between crossed polarisers.

3.2 Water stable isotope (δ^{18}O)

The stable oxygen isotope ratios (δ^{18}O) were measured in melted ice core sections, and in discrete under-ice water and brine samples. Samples for oxygen isotope composition were transferred into glass vials, filled completely and tightly capped with polyseal closures. Analysis was performed on a Picarro Isotopic Water Analyzer, L2120-/ (Picarro, Sunnyvale, USA) equipped with a PAL autosampler (Leap Technologies, Carrboro, USA). Details of the method can be found in Versteegh et al. (2012). Results are expressed in standard δ^{18}O notation using the V-SMOW standard as a reference. Agreement between triple consecutive injections of the same sample was usually within ±0.1 ‰.

3.3 Brine volume fraction and Rayleigh number

Brine volume (b) was calculated according to Cox and Weeks (1983) for ice temperatures $< -2\,^{\circ}$C and Leppäranta and Manninen (1988) for ice temperatures $\geq -2\,^{\circ}$C. Brine salinity (S_b) was calculated from the measured sea ice temperatures and the freezing point of seawater (Unesco, 1978). The brine volume fraction (V_b) was calculated as b/bulk sea ice volume (%).

The Rayleigh number is a parameter that determines the onset of convection (i.e. gravity drainage) and it provides information about the vertical stability within the brine

BGD
11, 4047–4083, 2014

inclusions. The Rayleigh number, *Ra*, following the definition of Notz and Worster (2009), for a given ice depth z, was estimated using:

$$Ra = \frac{g(h_i - z)\rho_w \beta_w [\sigma(z) - S_w]\pi(e_{min})}{\kappa_i \eta} \quad (1)$$

where g is the gravity acceleration $g = 9.81\,m\,s^{-2}$, $\sigma(z)$ is the brine salinity at the level z within the ice and S_w is the salinity of the sea water at the ice interface, so that $[\sigma(z) - S_w]$ express the salinity difference between the brine at the level z in the ice and seawater at the ice interface. ρ_w is the density of pure water, β_w is the haline expansion coefficient of seawater, both taken at 0 °C from Fofonoff (1985). $\pi(e_{min})$ is the effective ice permeability (m^2) computed using the formula of Freitag (1999) as a function of the minimum brine volume e_{min} between the level z in the ice cover and the ice–ocean interface. $\eta = 1.79 \times 10^{-3}\,kg\,m^{-1}\,s^{-1}$) is the dynamic viscosity of seawater at 0 °C. κ_i is the thermal diffusivity.

3.4 Total gas content

The total volume of gas within sea ice (content in mL STP of gas per kg of ice) was measured using the wet extraction method (Raynaud et al., 1988), at a resolution of 5 cm. Ice samples were placed in a glass container and then subjected to vacuum with a pressure of 10^{-2} torr. The ice was melted and then slowly refrozen at the bottom of the container using a −70 °C cold ethanol bath. This technique of melting and refreezing releases both the dissolved gas in the brine and the gas content from the bubbles in the headspace. After the refreezing, the container was connected to a Toepler pump for extraction (Raynaud et al., 1988).

3.5 The methane content

The methane from bulk sea ice ($[CH_4]_{bulk\ ice}$) was extracted using the wet extraction method (Raynaud et al., 1988) at 5 cm resolution. After refreezing, the headspace of

BGD
11, 4047–4083, 2014

the container contained both gas from the bubbles and the dissolved gas from the brines. The container was then connected to a gas chromatograph (Trace GC), which had a flame ionisation detector (FID) and equipped with a micro packed Shincarbon ST column (Skoog et al., 1997).

Concentrations of CH_4 from the seawater, $[CH_4]_{sw}$, and brines, $[CH_4]_{br}$, were determined by the technique described by Abril and Iversen (2002): a headspace of 30 mL of N_2 was created in the samples that was vigorously shaken and left overnight to ensure equilibration between melt water sample and the headspace before injecting into a gas chromatograph, SRI 8610C, equipped with a FID. $CH_4 : N_2$ mixtures (Air Liquide) of 1, 10 and 30 ppmv CH_4 were used as standards. The dissolved CH_4 concentrations were calculated using the solubility coefficient given by Yamamoto et al. (1976).

3.6 Bulk ice pCO_2 determination

The bulk ice pCO_2 was analyzed using a modification of the technique described by Geilfus et al. (2012b). The general principle of the method is to equilibrate the sea ice samples with a mixture of N_2 and CO_2 of known concentration (standard gas), at the in situ temperature and rapidly extract the gases into a GC under vacuum. The standard gas is injected at 1013 atm. into the headspace of a container containing the ice. The ice is cut to fit tightly into the container to both minimize the headspace volume and obtain a constant headspace volume. The container containing the ice and the standard gas is placed in a thermostatic bath for bringing the ice sample back to the in situ temperature. After 24 h, the sample is assumed to re-equilibrate to the brine volume and chemical conditions at the in situ temperature and partially in equilibrium with the standard gas. The air phase is then injected into vacuumed line linked to a gas chromatograph (Varian 3300, California, USA). The pressure difference between the vacuumed line and the container force all the remaining CO_2 (i.e. CO_2 not yet in equilibrium with the standard gas) to be rapidly extracted from the brine into the GC line. The method is only valid if the ice is permeable. We used a 550 ppmv standard for the equilibration process.

BGD
11, 4047–4083, 2014

3.7 Sea water pCO_2

The pCO_2 of brine and seawater from underneath the ice was measured in situ using a custom made equilibration system (Delille et al., 2007). The system consisted of a membrane contractor equilibrator (Membrana, Liqui-cell) that was connected to a non-dispersive infrared gas analyzer (IRGA, Li-Cor 6262, Nebraska, USA) via a closed air loop. Brine and airflow rates through respectively the equilibrator and IRGA were approximately 2 L min^{-1} and 3 L min^{-1}. Temperature was simultaneously measured in situ and at the outlet of the equilibrator using Li-Cor temperature sensors. Temperature correction of pCO_2 was applied assuming that the relation of Copin-Montégut (1988) is valid at low temperature and high salinity. Data were stored on a Li-Cor Li-1400 data logger. All the devices, except the peristaltic pump, were enclosed in an insulated box that contained a 12 V power source providing enough warming to keep the inside temperature just above 0 °C.

4 Results

4.1 Water column

Although the average fjord water salinity was 32.9, it dropped to below 2 at the ice–water interface (Fig. 2b, lower part). The $\delta^{18}O$ dropped from −0.957 ‰ at 1.09 m depth to −7.32 ‰ at the ice–water interface (Fig. 2c, lower part).

4.2 Sea ice

The sea ice thickness ranged from 62 cm to 66 cm. Except for a thin layer of granular ice at the top of the ice, the ice exclusively consisted of columnar ice indicating that ice growth occurred through quiet congelation of seawater at the ice–water interface (Eicken, 2003). We repeatedly observed tilted columnar ice crystal between 24 cm and

BGD
11, 4047–4083, 2014

32 cm suggesting the presence of a current at the ice–water interface during the ice growth (Fig. 3).

The bulk ice temperature ranged from −3.7 °C to −0.8 °C with the lowest values in the upper layers (Fig. 2a). The temperatures on 15 and 16 March were slightly higher than on 11 and 13 March. The averaged bulk ice salinity was 3.2 (Fig. 2b). Each profile exhibited a salinity profile that shifted from the typical C-shaped profile to a reversed S-shaped due to a drop of the salinity around 25 cm and 15 cm below the surface. The ice porosity profiles (i.e. brine volume fraction) were similar to those for the bulk ice salinity. For each, the brine volume fraction dropped under the permeability threshold of 5 % (Golden et al., 1998, 2007) at 25 cm and at 45 cm (Fig. 2d). During the survey, the brine network was therefore not fully connected preventing the internal fluid transport. The Rayleigh number (*Ra*), describing the probability that fluid transport occurs by convection within the brine network at a given depth in the sea ice, never exceeded 0.3 and therefore the expected critical convection threshold of 10 following Notz and Worster (2009) or 5 from Vancoppenolle et al. (2010) – (Fig. 2e) was not obtained during our study. During the four days, S_{ice} and V_b did not evolve and no temporal evolution trend was therefore observed.

The $\delta^{18}O$ ice isotopic composition ranged from −4 ‰ to −10 ‰ (Fig. 2c). The observed isotopic distributions displayed (1) depletion in heavy isotope at the same depth as the drop of the bulk ice salinity was observed (≈ 25 cm), and, (2) variation along the ice column greater than the maximum allowed by the fractionation coefficients. According to the literature (i.e. Eicken et al.,1998; Souchez et al., 1987, 1988), the fractionation rate depends on the freezing rate and on the thickness of the boundary layer. The fractionation coefficients at typical sea-ice growth velocities range from 1.5 ‰ and 2.5 ‰, with an equilibrium value (zero growth velocity) of around 2.7 ‰ (Eicken et al., 1998). On 11 March, the isotopic composition (18 to 22 cm) dropped from −5.5 ‰ to −9.2 ‰ (Δ = 3.7 ‰). On 15 March, the isotopic composition (22 to 26 cm) changed from −5.6 ‰ to −9.1 ‰ (Δ = 3.6 ‰). The fractionation process within sea ice itself could not explain these shifts.

BGD
11, 4047–4083, 2014

4.3 Gas content

4.3.1 Gas total

All values are below the expected content of Instant Freezing Sea Water (IFSW) (Cox and Weeks, 1983) and ranged between 4 and 21 mL STP kg^{-1} ice (Fig. 2f). A peak in gas content was observed between 25 cm and 35 cm. This peak was located where both the bulk ice salinity, and the brine volume fraction were at their lowest, and where the ice was depleted in $\delta^{18}O$.

4.3.2 Methane content

The concentration of dissolved CH_4 in the seawater ranged from 5.7 to 18.4 nmol L^{-1}, the maximum concentrations were measured at the ice–water interface (Fig. 4).

The bulk ice methane concentration, $[CH_4]_{bulk\ ice}$, ranged from 1.8 to 12.1 nmol L^{-1} (Fig. 3). The methane, as part of total gas volume (i.e. mixing ratio: $[CH_4]_{bulk\ ice}$ divided by the total gas content of the ice), ranged from 3 ppmv to 28 ppmv during the study, with an average value of 11.8 ppmv. The dissolved methane measured in the brine liquids, $[CH_4]_{br}$, ranged from 12 to 17.03 nmol L^{-1}.

4.3.3 Bulk ice pCO_2

The pCO_2 of the underlying seawater (below 0.5 m) was slightly under-saturated compared to the atmosphere (390 ppmv) and very under-saturated (77–130 ppmv) compared to seawater at the ice water interface. For the ice column, the average bulk ice pCO_2 was 194 ppmv. Except on 16 March the bulk ice pCO_2 increased from a minimum, lower than 185 ppmv, at the bottom of the ice to a maximum, exceeding 330 ppmv, in the top layers of the ice (Fig. 5).

BGD
11, 4047–4083, 2014

5 Discussion

5.1 Fresh water input at the ice–water interface

A thin surface layer with low salinities ($S_{surf} < 20$) and strong isotope depletion ($\delta^{18}O_{surf} < -8$ ‰) characterized the upper part of the water column. The low salinities and heavy isotope depletion could result from a dilution process, which implies a mixing of the fjord water with a water mass either from melting ice or from the Kapisillit River, or both. Assuming a conservative mixing between the three end members, the fraction of river water and the melting ice in the fjord water surface can be deduced from the following equations:

$$1 = f_{riv} + f_{ice} + f_{fjord} \quad (2)$$

$$S_{surf} = S_{riv} \times f_{riv} + S_{ice} \times f_{ice} + f_{fjord} \times S_{fjord} \quad (3)$$

$$\delta^{18}O_{surf} = f_{riv} \times \delta^{18}O_{riv} + f_{ice} \times \delta^{18}O_{ice} + f_{fjord} \times \delta^{18}O_{fjord} \quad (4)$$

Where f_{riv}, f_{ice} and f_{fjord} are the fraction of river water, melting ice and fjord water present at the surface of the fjord. S_{surf}, S_{fjord}, S_{riv} and S_{ice} are the salinity of the surface water ($S_{surf} < 20$), the fjord water at 9 m depth ($S_{fjord} = 32.9$), the river water (which is assumed to equal 0) and the bottom bulk ice salinity ($4.6 < S_{ice} < 8.8$). Where $\delta^{18}O_{surf}$, $\delta^{18}O_{riv}$, $\delta^{18}O_{ice}$ and $\delta^{18}O_{fjord}$ are the $\delta^{18}O$ content of the fjord surface layer (-6.44 ‰ $< \delta^{18}O_{surf} < -7.82$ ‰), the river water ($\delta^{18}O_{riv} = -14.84$ ‰), the bottom of the ice ($\delta^{18}O_{ice} = -4.55$ ‰) and the fjord water at 1.09 m depth ($\delta^{18}O_{fjord} = -0.957$ ‰). Following these equations the fraction of fresh water during the sampling period varies from 33 % to 50 % and water from the melting ice was less 2 %. This is in agreement with the study of Long et al. (2012) from the same area at the same period revealed low rates of ice melt at a maximum of 0.80 mm d^{-1}. As the river was unfrozen below its surface, we suggest that the stratification results of an input of fresh water from the Kapisillit river.

BGD
11, 4047–4083, 2014

5.2 Fresh water for earlier ice growth

In the previous section we have shown that freshwater from the Kapisillit river contribute to the low salinities close to the ice–water interface. During earlier ice growth, freshwater input may have produced similar changes of salinity, gas content, and isotope content into the water from which sea ice was formed. If no change had occurred in the parent water, we would expect that the isotopic composition of sea ice from the under-ice water monotonically shifts towards higher $\delta^{18}O$ values due to isotopic fractionation favouring the incorporation of heavy isotopes into the solid phase (ice) as compared to the liquid phase (Eicken et al., 1998; Souchez et al., 1988). Similarly, due to salt rejection during the freezing process, the salinity of sea ice is shifted towards lower salinities than the parent seawater. The salt rejection rate as well the isotopic fractionation depends mostly on the sea ice growth rate (Eicken, 2003). Once sea ice is formed, desalination occurs. The combination of salt segregation, gravity drainage and brine expulsion explains the typical "C-shape" of the salinity profiles, which evolve into the "I-shape" during the melting period (Eicken, 2003). The $\delta^{18}O$ profiles should however remain monotonically increasing downward, since most of the isotopic signal is recorded into the ice crystals themselves.

According to our data, the average bulk ice salinities (S_{ice}) of 3.2, was lower than typical values of first-year ice by a factor of 2 (Cox and Weeks, 1988; Eicken, 2003) and close to the bulk ice salinity ($2 < S_{ice} < 4.7$) of sea ice grown under influence of brackish water in the Laptev region of the Arctic Ocean (Eicken et al., 2005). The low S_{ice} induced a low brine volume fraction (V_b) that exceeded 10 % only in the bottom horizons of the ice and fell below the permeability threshold of 5 % (Golden et al., 1998, 2007) in the first 5 cm, between 20–30 cm, and at 45 cm depth (Fig. 5; dotted area). Thus, the brine network was stratified and not fully interconnected during the sampling period. Our measurements suggest that no fluid transport, by convective processes, could have taken place during the sampling period, since the Rayleigh numbers (*Ra*)

BGD
11, 4047–4083, 2014

were well below the threshold of 10 (Notz and Worster, 2009), or 5 (Vancopenolle et al., 2010).

Figure 6 shows a positive correlation between the bulk ice salinity and the isotope content between the 20–30 cm interval. The isotopic composition measured on bulk sea ice results from both a contribution of both brine and pure ice. Since the brine accounts for less than 10 % of the ice volume, the ice isotopic composition measured originates mainly from the pure ice. As no fractionation occurs in the solid phase during melting (Jouzel and Souchez, 1982), the $\delta^{18}O$ content in pure ice should not change over time and should depend only on processes occurring during freezing and on the composition of the underlying seawater (Eicken et al., 1998). On the other hand, the bulk ice salinity originates from the brine medium. Like the ice isotopic content, the bulk ice salinity depends on the ice growth velocities and on the composition of the underlying seawater. But once the ice is formed, desalination occurs. Sea ice looses salt primarily through brine drainage, convective transport, or flushing (Untersteiner, 1968). Since the bulk ice salinity is still correlated with the ice isotopic signal (Fig. 6; $R^2 = 0.64$, $p < 0.001$), it appears that no major desalinisation process have been active within the ice cover. Therefore, this ice should hold the original characteristics inherited from the parent water during the freezing process.

S-shaped profiles in the ice isotopic distribution and bulk ice salinity are uncommon and cannot be explained by the freezing or by desalinisation processes. Since the ice core samples were obtained before the onset of surface melt, and as there are no traces of either convective processes, melt water infiltration or superimposed ice in any of the samples it suggests that both the anomalies in the ice salinity profiles, and the heavy isotopic depletion in the ice, are mainly due to changes of water mass. We also note that the repeatedly oriented columnar ice crystal observed between 24 cm and 32 cm (Fig. 3) may suggest the presence of a current at the ice–water interface.

The bulk ice salinity and the ice isotope distribution can be used as proxy to track the salinity and the isotopic composition of the parent water, and hence indirectly quantify the fraction of river water. Thus, we may derive the fraction of river water present in

BGD
11, 4047–4083, 2014

a sea ice volume from isotope mass balance using the equation developed by Eicken et al. (2005):

$$f_{\mathrm{riv}} = \frac{\left[\delta^{18}\mathrm{O} - \varepsilon - \delta^{18}\mathrm{O}_{\mathrm{fjord}}\right]}{\left[\delta^{18}\mathrm{O}_{\mathrm{riv}} - \delta^{18}\mathrm{O}_{\mathrm{fjord}}\right]} \quad (5)$$

Where $\delta^{18}\mathrm{O}_{\mathrm{ice}}$, $\delta^{18}\mathrm{O}_{\mathrm{fjord}}$, $\delta^{18}\mathrm{O}_{\mathrm{riv}}$ are the isotopic composition of the ice, fjord water at 1.09 m depth, and river water, respectively. ε is the sea-ice fractionation coefficient ranging between 1.5 ‰ and 2.7 ‰ (Eicken et al., 1998). Since $\delta^{18}\mathrm{O}_{\mathrm{fjord}}$ and $\delta^{18}\mathrm{O}_{\mathrm{riv}}$ are constant over winter (November to April) (Fitzner et al., 2014) we can determine the temporal changes in surface water composition, namely the fraction of river water f_{riv} and the salinity of the surface parent water mass S_{p}. According to Eicken et al. (2005), S_{p} is given as:

$$S_{\mathrm{p}} = (1 - f_{\mathrm{riv}}) \times S_{\mathrm{fjord}} \quad (6)$$

The maximum f_{riv} deduced from the ice isotopic mass balance occurs when the sea ice reached a thickness of between 20 and 30 cm. The computed salinity shows that at this time S_{p} had to drop by a factor of 1.7 and could not exceed 18. This shift probably induced the drop in bulk ice salinity in the horizon at 25 cm below the surface.

5.3 Gas content and fresh water input

The total gas content was always lower than the 23.75 mL STP kg^{-1} value expected in IFSW (Cox and Weeks, 1983). This is in agreement with previous reports that gases in seawater are preferentially expelled from the growing ice as for other impurities (Cox and Weeks, 1983, 1988; Killawee et al., 1998; Loose et al., 2009, 2011; Tison et al., 2002). The range of total gas-content values for all the samples was 4–21 mL STP kg^{-1}, which is comparable to the range obtained by Matsuo and Miyake (1966) for natural sea ice (2.2–21.2 mL STP kg^{-1}) and the range of 3–18 mL STP kg^{-1}

BGD
11, 4047–4083, 2014

obtained by Tison et al. (2002) for artificial sea ice. In this study there was a peak of gas content between 25 cm and 35 cm associated with the lowest salinities. As we demonstrated above, the change of salinity was caused by a change in the parent water due to an input of fresh water. By computing f_{riv} and S_p during the ice growing period, we can further assess the freezing temperature of the parent ice water, following the equation of Weeks (2010). Based on the salinities and temperatures of the surface waters, we can compute the gas content of the surface parent water at each stage of ice growth using the solubility law given by Garcia and Gordon (1992) for O_2, and Hamme and Emerson (2004) for N_2 and Ar. When the ice reached a thickness of 25 cm, the salinity of the parent water decreased by a factor of 1.7, increasing the gas solubility by a factor 1.05, although the sea ice gas content had been increased by a factor of 2.1. The increasing gas-content in the parent water, dictated by the increasing solubility could not alone explain the gas peak in the middle horizons of the ice. Tison et al. (2002) showed that the initial gas content of sea ice affected by a current at the ice water interface that was 3 times higher than the gas-content of sea ice grown with a stagnant water–ice interface. According to Tison et al. (2002), the current zone is characterized by a thinner boundary layer in which both salts and gases are controlled by diffusion. Due to this thin boundary layer, the current zone reaches the critical value necessary for early bubble nucleation. Once started, bubble nucleation ensures that that the gasses that would otherwise have diffused as a solute towards the water will be entrapped as bubbles in the sea ice. Moreover, the total gas content depends on the ice growth velocities while fresh water grow faster than salty water, more gases were trapped into the sea ice cover. Thus, we propose that the peak in sea ice gas content is a result of the increasing gas content in the parent water and the presence of a current under the sea ice interface; both caused by a flux of fresh water.

BGD
11, 4047–4083, 2014

5.4 Greenhouse gases in sea ice

5.4.1 Methane

The methane concentration was measured in the water column $[CH_4]_{sw}$, in the ice cover $[CH_4]_{bulk\ ice}$ and in the brine medium $[CH_4]_{br}$. First, we compare $[CH_4]_{sw}$ and $[CH_4]_{bulk\ ice}$ with the methane concentration at saturation; $[CH_4]_{sat\ sw}$ and $[CH_4]_{sat\ bulk\ ice}$. The concentration at saturation is the concentration of methane dissolved in a liquid (i.e. brine or seawater) in equilibrium with the atmospheric partial pressure of methane. The saturation is determined by the solubility, which depends on the temperature and salinity. CH_4 saturation with respect to the atmosphere at the sea surface was calculated assuming a 2010 atmospheric mixing ratio of 1.9 ppmv, using the CH_4 solubility equation of Wiesenburg and Guinasso (1979) corrected for the in situ temperature and salinity. We assumed that the relationships from the reference are valid for the range of temperature and salinity found in the ice. The bulk ice saturation $[CH_4]_{sat\ bulk\ ice}$ was obtained by multiplying the calculated solubility in brine (nmol L^{-1} brine) by the relative brine volume (L brine L^{-1} bulk ice). The ratio between the observed $[CH_4]_{bulk\ ice}$ to the $[CH_4]_{sat\ bulk\ ice}$ determines the supersaturation factor.

According to Weisemburg and Guinasso (1979), the methane concentration in equilibrium with the atmospheric pressure for seawater salinities > 33.9 and a temperature of −1.9 °C is 3 to 4 nmol L^{-1}. Thus, the dissolved methane in the surface water was 4.5 times the concentration at saturation (i.e 450 % supersaturated). Such high concentrations, up to 15 nmol L^{-1}, suggest that the top layer was somehow affected by near-sources (i.e. sediment degassing, riverine input). These observations are similar to the values (5–55 nmol L^{-1} water) reported by Damm et al. (2007) in Storfjorden (Svalbard Archipelago) and in the fjords of Spitsbergen (Damm et al., 2005). The observed concentrations are, however, lower than the concentration in East Siberian Arctic Shelf (ESAS) observed by Shakova et al. (2010). Due to the thawing subsea permafrost, CH_4 – rich bubbles released from the sea floor rise up through the water column. As far as

BGD
11, 4047–4083, 2014

we aware no subsea thawing permafrost has been reported in Gothabsfjord. Damm et al. (2008) suggest than methane plumes in the water come from sediments during winter and from in situ production during phytoplankton bloom during the summer. As our studies took place before the algal bloom, one of the main methane sources should be the sediment. The methane released from sediments raises trough the water column by convective processes and accumulates under the ice. However, we have to consider the Kapissilit river that runs through a fen (Jensen and Racsh, 2011) as potential source of dissolved methane at the surface of the water column. The fen in the fjord area is a source of CH_4 due to the permanently wet conditions that promote anaerobic decomposition, by which CH_4 is an end product (Jensen and Racsh, 2011).

The range of CH_4 concentrations in the bulk ice (1.8–12.1 nmol L^{-1} ice) is in agreement with the observation (15 to 25 nmol L ice) reported by Lorenson and Kvenolden (1995) and Zhou et al. (2014). The deduced mixing ratio ranges between 3 ppmv to 28 ppmv indicates that the methane content within sea ice was consistently higher than the atmospheric concentration (1.9 ppmv). The ice cover exceeded the concentrations at atmospheric saturation with saturation state ranging from 1200 % to 70 000 % with an average saturation level of 2400 %. Thus, sea ice could plausibly act as an atmospheric methane source.

First, we compare $[CH_4]_{bulk\ ice}$ with $[Ar]_{bulk\ ice}$ (bulk ice Ar, O_2, N_2 were measured by gas chromatography and the profiles are discussed in Crabeck et al. (2014). As the diffusion process controls the gas motion within the sea ice Crabeck et al. (2014), Ar can be used as a tracer of physical processes. In marine biology, the O_2 : Ar ratio is commonly used to remove the physical contribution to oxygen super-saturation for determining the biological oxygen production. Our CH_4 samples were randomly distributed related to the Ar ($R^2 \leq 0.21$, $p < 0.01$; Fig. 7). The CH_4 : Ar ratio was systematically higher than the atmospheric and seawater ratios. Hence, CH_4 has been preferentially accumulated within the sea ice cover relative to Ar. This could be related to in situ biological production. Since methane is produced by methanogen bacteria and requires anoxic conditions. DNA (deoxyribonucleic acid) from methanogen archaea as well as

BGD
11, 4047–4083, 2014

anaerobic pathway has been observed in Arctic sea ice (Collins et al., 2010; Rysgaard et al., 2004). Firstly, high-resolution O_2 measurements in the Kapisillit sea ice show no anoxic condition during the sampling period (Crabeck et al., 2014). Secondly, denitrification, which is an anaerobic process requiring less energy than methanogenis was not active within the sea ice due to presence of oxygen. In addition, the ratio $Ar : N_2$, showed no significant deviations to the sea water ratio (Fig. 7). Therefore we conclude that the methane accumulation was not related to biological in situ production. We suggest that the accumulation of methane was due to (1) the initial CH_4 concentration in the seawater and (2) the bubble formation that can act as a methane trap. Assuming a steady rate of incorporation for each gas, the accumulation and super-saturation (up to 450 %) of CH_4 in the surface water leads to a larger incorporation of CH_4 in the ice, and consequently greater CH_4 accumulation relative to Ar. The bulk ice methane concentration ($[CH_4]_{bulk\ ice}$) represents the total methane content within the sea ice as the sum of the dissolved methane in the brine medium ($[CH_4]_{br}$) and the methane trapped in bubbles ($[CH_4]_{bubbles}$). We can deduce the fraction of the methane trapped in bubbles, $f_{[CH_4]_{bubbles}}$, using the following relationships:

$$[CH_4]_{bulk\ ice} = [CH_4]_{bubbles} + [CH_4]_{br} \quad (7)$$

$$f_{[CH_4]_{bubbles}} = \left(\frac{([CH_4]_{bulk\ ice} - [CH_4]_{br})}{[CH_4]_{bulk\ ice}} \right) \times 100 \quad (8)$$

Based on these relationships, the trapped methane bubbles contributed up to 70 % of the sea ice methane content. According to our estimates, methane bubbles were preferentially accumulated in the upper layers of the sea ice. We pinpoint three sources of methane bubbles; (1) the methane bubbles trapped during the freezing process and (2) the in situ formation of methane bubbles within the brine medium and (3) ebullition from degassing sediment. Add (1): during seawater freezing, dissolved solutes (ions and gases) are segregated from the ice matrix (Cox and Weeks, 1983; Killawee et al., 1998; Understeiner, 1968) and become concentrated in the liquid near the freezing

BGD
11, 4047–4083, 2014

interface. As the partial pressures of gases increases beneath growing ice, bubbles nucleate and are included along ice crystal boundaries (Bari and Hallett, 1974; Cox and Weeks, 1983; Killawee et al., 1998; Tison et al., 2002). Taking into account, that the surface water is initially supersaturated with CH_4, the value to trigger the nucleation process, has been reached earlier than for the other gases. Thus, the growing ice has been enriched in methane by bubble formation that would otherwise have diffused as a solute towards the water reservoir (Tison et al., 2002). Add (2): as the sea ice temperature decreases, brine becomes further concentrated and supersaturated and gases can nucleate from the solution (Killawee et al., 1998; Tison et al., 2002). As CH_4 has the lowest solubility (Weisemburg and Guinasso, 1979), bubble formation had to be triggered first. Once formed, the bubbles can only migrate upward due to their buoyancy until they are blocked under the impermeable layer or released into the atmosphere. In contrast the dissolved species in the brines medium can diffuse to the underlying seawater. Hence, bubble formation leads to an accumulation of CH_4 inside the ice cover. The upward migration of the bubble could partially explain the preferential bubble accumulation in the top 20 cm of the ice column, a process recently discussed for the Ar in Zhou et al. (2013) and modelled by Moreau et al. (2014). Add (3): lastly, bubbles could directly come from the degassing sediment and be trapped in the growing sea ice cover. This phenomenon has been observed by Shakova et al. (2010) in the East Siberian Arctic Shelf. Unfortunately our data set does not provide any proof to the potential ebullition process from the sea floor.

5.4.2 pCO_2

The pCO_2 of the water column is slightly undersaturated (354–384 ppmv) compared to the atmosphere (390 ppmv), whereas at the ice–water interface the pCO_2 is largely under saturated (77–130 ppmv). As noted above, the thin surface layer is under the influence of a mixing processes, which could produced a drop of the water pCO_2 at ice–water interface. Moreover, the annual monitoring measurements provided by the

BGD
11, 4047–4083, 2014

Nuuk Ecological Research Operations (Jensen and Rasch, 2011) observed year-round pCO_2 subsatured surface water in the Gothabsfjord system.

The range of 77–330 ppmv and average of 194 ppmv for the bulk ice pCO_2 is in the same range as the profiles of bulk sea ice pCO_2 measured on natural and experimental sea ice (Geilfus et al., 2012a). According to Geilfus et al. (2012a, b) and Delille et al. (2007) the bulk ice pCO_2 is under-saturated once ice temperature is above −4 °C. One of the main factors controlling the inorganic carbon dynamics within sea ice appears to be temperature. Indeed, as temperature increased, the subsequent decrease of the salinity promotes the brine dilution and a decrease of the brine pCO_2. According to our data, the bulk ice pCO_2 is inversely correlated to the ice temperature. Indeed, the high values of bulk ice pCO_2 (up 330 ppmv) are associated with the coldest temperature (−3 to −4 °C) and as the temperature increases with the ice thickness, the bulk ice pCO_2 decreases to ≈ 100 ppmv −190 ppmv and reach the same range of pCO_2 concentration as the underlying seawater, ≈ 76–130 ppmv.

Other processes affect the pCO_2 concentrations within sea ice such as the precipitation and dissolution of calcium carbonate (Dieckmann et al., 2008; Geilfus et al., 2012b, 2013a, b; Rysgaard et al., 2007, 2011, 2013). During the sea ice melt the carbonate dissolution promotes lower pCO_2 conditions (Rysgaard et al., 2011). Søgaard et al. (2013) suggested that the main factor controlling the total alkalinity and the dissolved inorganic carbon of the sea ice of Kapisillit was the dissolution of calcium carbonate crystals. Hence, the dissolution of calcium carbonates, associated with the high temperature and the subsequent decrease of salinity was likely the reason for the observed low bulk ice pCO_2 during our study also.

Finally, the biological activity as primary production as well bacterial respiration can affect the inorganic carbon dynamics within sea ice (Delille et al., 2007; Kaartokallio et al., 2013; Rysgaard et al., 2007, 2009; Søgaard et al., 2013). Ice melting through spring and summer will produce both a continuous reduction of the bulk ice pCO_2 and an increase of the ice permeable features leading to pCO_2 subsaturated sea ice relative to the atmosphere and hereby enhance the air–sea flux of CO_2,

BGD
11, 4047–4083, 2014

6 Conclusions

The freshwater runoff from the surrounding land influenced the sea ice during formation, and was evident as a thin freshwater layer at the sea ice-water column interface. Sea ice was influenced by riverine input during ice growth. This caused deviation from the traditional C-shaped ice salinity profile and depletion in heavy isotope of the sea ice cover. Moreover, the low bulk ice salinity induced a stratified brine network, which prevented the convective exchange between the ice, the water and the atmosphere. The freshwater, also potentially triggered by higher temperatures and/or storms, caused increased buoyancy and currents velocities at the sea ice–water interface, which would have accelerated the nucleation processes in the boundary layer and consequently increased the total gas content of the ice.

The partial pressure of CH_4 exceeded the atmospheric CH_4 content and sea ice can potentially be a source of CH_4 for the atmosphere. During periods of sea ice cover, CH_4 can accumulate within or below the sea ice, and when the ice breaks up and melts during spring and summer, large CH_4 fluxes to the atmosphere could be expected. During sea ice break-up, Gosink and Kelley (1979) and Shakova et al. (2010) observed an increase CH_4 concentration in the atmosphere above sea ice as well as in surface seawaters.

While the CH_4 from the seawater is accumulated within the sea ice cover, the sea cover provides an interface in which the methane could be stored and transformed over time by biogeochemical processes. Further studies based on longer times series and carbon isotope signatures $\delta^{13}CH_4$ will provide us the opportunity to study the potential methane oxidation rate within the sea ice cover. In the case of the CH_4 being oxidised over time within the sea ice cover, the sea ice could provide an interface where CH_4 is degraded and, hence, act as sink for oceanic CH_4.

We achieve a value for the bulk ice pCO_2 measured of an average 194 ppmv. Thus, the upper layer of the sea-ice cover was greatly subsatured compared to the atmosphere and it should be expected that the air to sea flux of CO_2 will increase when sea

BGD
11, 4047–4083, 2014

ice starts to melt. Our study adds to the few existing studies of CH_4 and CO_2 in sea ice and concludes that sub-arctic sea can be a sink for atmospheric CO_2, while being a net source of CH_4.

Acknowledgements. We gratefully acknowledge the contributions of the Canada Excellence Research Chair (CERC) and Canada Research Chair (CRC) programs. Support was also provided by the Natural Sciences and Engineering Research (NSERC) Council, the Canada Foundation for Innovation and the University of Manitoba. This work is a contribution to the ArcticNet Networks of Centres of Excellence and the Arctic Science Partnership (ASP) asp-net.org. This work is also a contribution to the Belgian FNRS-FRFC 2.4584.09 research contract. BD is a research associate of F.R.S.-FNRS. The authors would like to thank Saïda El Amri for her efficient help in laboratory work.

References

Abril, G. and Iversen, N.: Methane dynamics in a shallow non-tidal estuary (Randers Fjord, Denmark), Mar. Ecol.-Prog. Ser., 230, 171–181, doi:10.3354/meps230171, 2002.

Bari, S. A. and Hallet, J.: Nucleation and growth of bubbles at an ice–water interface, J. Glaciol., 13, 489–520, 1974.

Bates, N. R. and Mathis, J. T.: The Arctic Ocean marine carbon cycle: evaluation of air-sea CO_2 exchanges, ocean acidification impacts and potential feedbacks, Biogeosciences, 6, 2433–2459, doi:10.5194/bg-6-2433-2009, 2009.

Collins, R. E., Rocap, G., and Deming, J. W.: Persistence of bacterial and archaeal communities in sea ice through an Arctic winter, Environ. Microbiol., 12, 1828–1841, doi:10.1111/j.1462-2920.2010.02179.x, 2010.

Copin Montégut, C.: A new formula for the effect of temperature on the partial pressure of carbon dioxide in seawater, Mar. Chem., 25, 29–37, 1988.

Cox, G. F. N. and Weeks, W. F.: Equations for determining the gas and brine volumes in sea-ice samples, J. Glaciol., 29, 306–316, 1983.

Cox, G. F. N. and Weeks, W. F.: Numerical simulations of the profile properties of undeformed 1st-year sea ice during the growth season, J. Geophys. Res.-Oceans, 93, 12449–12460, doi:10.1029/JC093iC10p12449, 1988.

BGD
11, 4047–4083, 2014

Crabeck, O., Delille, B., Rysgaard, S., Thomas, D., Geilfus, N. X., Else, B., and Tison, J. L.: First "in situ" determination of gas transport coefficients (D_{O_2}, D_{Ar} and D_{N_2}) from bulk gas concentration measurements (O_2, N_2, Ar) in natural sea ice, J. Geophys. Res., submitted, 2014.

Damm, E., Mackensen, A., Budeus, G., Faber, E., and Hanfland, C.: Pathways of methane in seawater: plume spreading in an Arctic shelf environment (SW-Spitsbergen), Cont. Shelf. Res., 25, 1453–1472, doi:10.1016/j.csr.2005.03.003, 2005.

Damm, E., Schauer, U., Rudels, B., and Haas, C.: Excess of bottom-released methane in an Arctic shelf sea polynya in winter, Cont. Shelf. Res., 27, 1692–1701, doi:10.1016/j.csr.2007.02.003, 2007.

Damm, E., Kiene, R. P., Schwarz, J., Falck, E., and Dieckmann, G.: Methane cycling in Arctic shelf water and its relationship with phytoplankton biomass and DMSP, Mar. Chem., 109, 45–59, doi:10.1016/j.marchem.2007.12.003, 2008.

Damm, E., Helmke, E., Thoms, S., Schauer, U., Nöthig, E., Bakker, K., and Kiene, R. P.: Methane production in aerobic oligotrophic surface water in the central Arctic Ocean, Biogeosciences, 7, 1099–1108, doi:10.5194/bg-7-1099-2010, 2010.

Delille, B., Jourdain, B., Borges, A. V., Tison, J. L., and Delille, D.: Biogas (CO_2, CO_2, dimethylsulfide) dynamics in spring Antarctic fast ice, Limnol. Oceanogr., 52, 1367–1379, 2007.

Dieckmann, G. S., Nehrke, G., Papadimitriou, S., Gottlicher, J., Steininger, R., Kennedy, H., Wolf-Gladrow, D., and Thomas, D. N.: Calcium carbonate as ikaite crystals in Antarctic sea ice, Geophys. Res. Lett., 35, L08501, doi:10.1029/2008GL033540, 2008.

Eicken, H.: From the microscopic to the macroscopic to the regional scale, growth, microstrucutre and properties of sea ice, in: Sea Ice – an Introduction to Its Physics, Biology, Chemistry and Geology, Blackwell Science, London, 22–81, 2003.

Eicken, H., Lange, M. A., and Dieckmann, G. S.: Spatial variability of sea ice properties in the Northwestern Weddell Sea, J. Geophys. Res.-Oceans, 96, 10603–10615, 1991.

Eicken, H., Weissenberger, J., Bussmann, I., Freitag, J., Schuster, W., Delgado, F. V., Evers, K. U., Jochmann, P., Krembs, C., Gradinger, R., Lindemann, F., Cottier, F., Hall, R., Wadhams, P., Reisemann, M., Kousa, H., Ikavalko, J., Leonard, G. H., Shen, H., Ackley, S. F., and Smedsrud, L. H.: Ice-tank studies of physical and biological sea-ice processes, in: Ice in Surface Waters, vol. 1, edited by: Shen, H. T., 363–370, 1998.

BGD
11, 4047–4083, 2014

Eicken, H., Dmitrenko, I., Tyshko, K., Darovskikh, A., Dierking, W., Blahak, U., Groves, J., and Kassens, H.: Zonation of the Laptev Sea landfast ice cover and its importance in a frozen estuary, Global Planet. Change, 48, 55–83, doi:10.1016/j.gloplacha.2004.12.005, 2005.

Fitzner, A., van As, D., Bendtsen, J., Dahl-Jensen, D., Fettweis, X., Mortensen, J., and Rysgaard, S.: Estimating the glacial meltwater contribution to the freshwater budget from salinity and $\delta^{18}O$ measurements in Godthåbsfjord, J. Geophys. Res., submitted, 2014.

Fofonoff, N. P.: Physical-properties of seawater – a new salinity scale and equation of state for seawater, J. Geophys. Res.-Oceans, 90, 3332–3342, doi:10.1029/JC090iC02p03332, 1985.

Freitag, J.: Untersuchungen zur Hydrologie des arktischen Meereises – Konsequenzen für den kleinskaligen Stofftransport, Ber. Polarforsch./Rep. Pol. Res., 325, 1999.

Garcia, H. E. and Gordon, L. I.: Oxygen solubility in seawater – better fitting equations, Limnol. Oceanogr., 37, 1307–1312, 1992.

Geilfus, N. X., Carnat, G., Papakyriakou, T., Tison, J. L., Else, B., Thomas, H., Shadwick, E., and Delille, B.: Dynamics of pCO_2 and related air–ice CO_2 fluxes in the Arctic coastal zone (Amundsen Gulf, Beaufort Sea), J. Geophys. Res.-Oceans, 117, C00g10, doi:10.1029/2011jc007118, 2012a.

Geilfus, N. X., Delille, B., Verbeke, V., and Tison, J. L.: Towards a method for high vertical resolution measurements of the partial pressure of CO_2 within bulk sea ice, J. Glaciol., 58, 287–300, doi:10.3189/2012JoG11J071, 2012b.

Geilfus, N. X., Carnat, G., Dieckmann, G. S., Halden, N., Nehrke, G., Papakyriakou, T., Tison, J. L., and Delille, B.: First estimates of the contribution of $CaCO_3$ precipitation to the release of CO_2 to the atmosphere during young sea ice growth, J. Geophys. Res., 118, 244–255, doi:10.1029/2012JC007980, 2013a.

Geilfus, N. X., Galley, R. J., Cooper, M., Halden, N., Hare, A., Wang, F., Søgaard, D. H., and Rysgaard, S.: Gypsum crystals observed in experimental and natural sea ice, Geophys. Res. Lett., 40, 6362–6367, doi:10.1002/2013GL058479, 2013b.

Gleitz, M., Vonderloeff, M. R., Thomas, D. N., Dieckmann, G. S., and Millero, F. J.: Comparison of summer and winter inorganic carbon, oxygen and nutrient concentrations in antarctic sea-ice brine, Mar. Chem., 51, 81–91, doi:10.1016/0304-4203(95)00053-t, 1995.

Golden, K. M., Ackley, S. F., and Lytle, V. I.: The percolation phase transition in sea ice, Science, 282, 2238–2241, 1998.

BGD
11, 4047–4083, 2014

Golden, K. M., Eicken, H., Heaton, A. L., Miner, J., Pringle, D. J., and Zhu, J.: Thermal evolution of permeability and microstructure in sea ice, Geophys. Res. Lett., 34, L16501, doi::10.1029/2007GL030447, 2007.

Gosink, T. A. and Kelley, J. J.: Carbon-monoxide evolution from arctic surfaces during spring thaw, J. Geophys. Res.-Oc. Atm., 84, 7041–7041, doi:10.1029/JC084iC11p07041, 1979.

Hamme, R. C. and Emerson, S. R.: Measurement of dissolved neon by isotope dilution using a quadrupole mass spectrometer, Mar. Chem., 91, 53–64, doi:10.1016/j.marchem.2004.05.001, 2004.

Jensen, L. M. and Rasch, M. (Eds.): NERO – Nuuk Ecological Reseach Operations, 3rd Annual Report 2010, Roskilde, National Environmental Research Institute, Aarhus University, Aarhus, 2011.

Jouzel, J. and Souchez, R. A.: Melting refreezing at the glacier sole and the isotopic composition of the ice, J. Glaciol., 28, 35–42, 1982.

Kaartokallio, H., Sogaard, D. H., Norman, L., Rysgaard, S., Tison, J. L., Delille, B., and Thomas, D. N.: Short-term variability in bacterial abundance, cell properties, and incorporation of leucine and thymidine in subarctic sea ice, Aquat. Microb. Ecol., 71, 57–73, doi:10.3354/ame01667, 2013.

Killawee, J. A., Fairchild, I. J., Tison, J. L., Janssens, L., and Lorrain, R.: Segregation of solutes and gases in experimental freezing of dilute solutions: implications for natural glacial systems, Geochim. Cosmochim. Ac., 62, 3637–3655, 1998.

Kitidis, V., Upstill-Goddard, R. C., and Anderson, L. G.: Methane and nitrous oxide in surface water along the North-West Passage, Arctic Ocean, Mar. Chem., 121, 80–86, doi:10.1016/j.marchem.2010.03.006, 2010.

Kort, E. A., Wofsy, S. C., Daube, B. C., Diao, M., Elkins, J. W., Gao, R. S., Hintsa, E. J., Hurst, D. F., Jimenez, R., Moore, F. L., Spackman, J. R., and Zondlo, M. A.: Atmospheric observations of Arctic Ocean methane emissions up to 82 degrees north, Nat. Geosci., 5, 318–321, doi:10.1038/ngeo1452, 2012.

Kvenvolden, K. A., Lilley, M. D., Lorenson, T. D., Barnes, P. W., and McLaughlin, E.: The beaufort sea continental-shelf as a seasonal source of atmospheric methane, Geophys. Res. Lett., 20, 2459–2462, doi:10.1029/93gl02727, 1993.

Langway, C. C.: Ice fabrics and the universal stage Rep. 62, US Snow, Ice and 496 Permafrost Research Establishment, Wilmette, Illinois, 1958.

BGD
11, 4047–4083, 2014

Leppäranta, M. and Manninen, T.: The brine and gas content of sea ice with attention to low salinities and high temperatures, Helsinki, 1988.
Long, M. H., Koopmans, D., Berg, P., Rysgaard, S., Glud, R. N., and Søgaard, D. H.: Oxygen exchange and ice melt measured at the ice-water interface by eddy correlation, Biogeosciences, 9, 1957–1967, doi:10.5194/bg-9-1957-2012, 2012.
Loose, B., McGillis, W. R., Schlosser, P., Perovich, D., and Takahashi, T.: Effects of freezing, growth, and ice cover on gas transport processes in laboratory seawater experiments, Geophys. Res. Lett., 36, L05603, doi:10.1029/2008gl036318, 2009.
Loose, B., Schlosser, P., Perovich, D., Ringelberg, D., Ho, D. T., Takahashi, T., Richter-Menge, J., Reynolds, C. M., McGillis, W. R., and Tison, J. L.: Gas diffusion through columnar laboratory sea ice: implications for mixed-layer ventilation of CO_2 in the seasonal ice zone, Tellus B, 63, 23–39, doi:10.1111/j.1600-0889.2010.00506.x, 2011.
Matsuo, S. and Miyake, Y.: Gas composition in ice samples from Antarctica, J. Geophys. Res., 71, 5235–5241, 1966.
Moreau, S., Vancoppenolle, M., Zhou, J. Y., Tison, J. L., Delille, B., and Goosse, H.: Modelling argon dynamics in first-year sea ice, Ocean Model., 73, 1–18, doi:10.1016/j.ocemod.2013.10.004, 2014.
Nomura, D., Yoshikawa-Inoue, H., and Toyota, T.: The effect of sea-ice growth on air–sea CO_2 flux in a tank experiment, Tellus B, 58, 418–426, 2006.
Nomura, D., Eicken, H., Gradinger, R., and Shirasawa, K.: Rapid physically driven inversion of the air–sea ice CO_2 flux in the seasonal landfast ice off Barrow, Alaska after onset surface melt, Cont. Shelf. Res., 30, 1998–2004, 2010.
Nomura, D., Granskog, M. A., Assmy, P., Simizu, D., and Hashida, G.: Arctic and Antarctic sea ice acts as a sink for atmospheric CO_2 during periods of snowmelt and surface flooding, J. Geophys. Res.-Oceans, 118, 6511–6524, doi:10.1002/2013JC009048, 2013.
Notz, D. and Worster, M. G.: Desalination processes of sea ice revisited, J. Geophys. Res., 114, C05006, doi:10.1029/2008JC004885, 2009.
Parmentier, F.-J. W., Christensen, T. R., Sørensen, L. L., Rysgaard, S., McGuire, A. D., Miller, P. A., and Walker, D. A.: The impact of lower sea-ice extent on Arctic greenhouse-gas exchange, Nature Clim. Change, 3, 195–202, doi:10.1038/NCLIMATE1784, 2013.
Ramaswamy, V., Chanin, M. L., Angell, J., Barnett, J., Gaffen, D., Gelman, M., Keckhut, P., Koshelkov, Y., Labitzke, K., Lin, J. J. R., O'Neill, A., Nash, J., Randel, W., Rood, R., Shine, K.,

BGD
11, 4047–4083, 2014

Shiotani, M., and Swinbank, R.: Stratospheric temperature trends: observations and model simulations, Rev. Geophys., 39, 71–122, doi:10.1029/1999rg000065, 2001.
Raynaud, D., Chappellaz, J., Barnola, J. M., Korotkevich, Y. S., and Lorius, C.: Climatic and CH_4 cycle implications of glacial interglacial CH_4 change in the Vostok ice core, Nature, 333, 655–657, doi:10.1038/333655a0, 1988.
Rysgaard, S. and Glud, R. N.: Anaerobic N_2 production in Arctic sea ice, Limnol. Oceanogr., 49, 86–94, 2004.
Rysgaard, S., Glud, R. N., Sejr, M. K., Bendtsen, J., and Christensen, P. B.: Inorganic carbon transport during sea ice growth and decay: a carbon pump in polar seas, J. Geophys. Res.-Oceans, 112, C03016, doi:10.1029/2006JC003572, 2007.
Rysgaard, S., Bendtsen, J., Delille, B., Dieckmann, G. S., Glud, R. N., Kennedy, H., Mortensen, J., Papadimitriou, S., Thomas, D. N., and Tison, J. L.: Sea ice contribution to the air–sea CO_2 exchange in the Arctic and Southern Oceans, Tellus B, 63, 823–830, doi:10.1111/j.1600-0889.2011.00571.x, 2011.
Rysgaard, S., Søgaard, D. H., Cooper, M., Pućko, M., Lennert, K., Papakyriakou, T. N., Wang, F., Geilfus, N. X., Glud, R. N., Ehn, J., McGinnis, D. F., Attard, K., Sievers, J., Deming, J. W., and Barber, D.: Ikaite crystal distribution in winter sea ice and implications for CO_2 system dynamics, The Cryosphere, 7, 707–718, doi:10.5194/tc-7-707-2013, 2013.
Savvichev, A. S., Rusanov, II, Yusupov, S. K., Pimenov, N. V., Lein, A. Y., and Ivanov, M. V.: The biogeochemical cycle of methane in the coastal zone and littoral of the Kandalaksha Bay of the White Sea, Microbiology+, 73, 457–468, doi:10.1023/B:MICI.0000036992.80509.2a, 2004.
Semiletov, I. P., Makshtas, A., Akasofu, S. I., and Andreas, E. L.: Atmospheric CO_2 balance: the role of Arctic sea ice, Geophys. Res. Lett., 31, L05121, doi:10.1029/2003GL017996, 2004.
Shakhova, N., Semiletov, I., Leifer, I., Salyuk, A., Rekant, P., and Kosmach, D.: Geochemical and geophysical evidence of methane release over the East Siberian Arctic Shelf, J. Geophys. Res.-Oceans, 115, C08007, doi:10.1029/2009jc005602, 2010.
Skoog, D. A., West, D. M., and Holler, F. J.: Chimie Analytique, De Boeck Université, 552 Paris, Bruxelles, 1997.
Sogaard, D. H., Thomas, D. N., Rysgaard, S., Glud, R. N., Norman, L., Kaartokallio, H., Juul-Pedersen, T., and Geilfus, N. X.: The relative contributions of biological and abiotic processes to carbon dynamics in subarctic sea ice, Polar Biol., 36, 1761–1777, doi:10.1007/s00300-013-1396-3, 2013.

BGD
11, 4047–4083, 2014

Souchez, R., Tison, J. L., and Jouzel, J.: Freezing rate determination by the isotopic composition of the ice, Geophys. Res. Lett., 14, 599–602, doi:10.1029/GL014i006p00599, 1987.
Souchez, R., Tison, J. L., and Jouzel, J.: Deuterium concentration and growth-rate of antarctic 1st-year sea ice, Geophys. Res. Lett., 15, 1385–1388, doi:10.1029/GL015i012p01385, 1988.
Takahashi, T., Sutherland, S. C., Wanninkhof, R., Sweeney, C., Feely, R. A., Chipman, D. W., Hales, B., Friederich, G., Chavez, F., Sabine, C., Watson, A., Bakker, D. C. E., Schuster, U., Metzl, N., Yoshikawa-Inoue, H., Ishii, M., Midorikawa, T., Nojiri, Y., Kortzinger, A., Steinhoff, T., Hoppema, M., Olafsson, J., Arnarson, T. S., Tilbrook, B., Johannessen, T., Olsen, A., Bellerby, R., Wong, C. S., Delille, B., Bates, N. R., and de Baar, H. J. W.: Climatological mean and decadal change in surface ocean pCO_2, and net sea–air CO_2 flux over the global oceans, Deep-Sea Res. Pt. II, 56, 554–577, doi:10.1016/j.dsr2.2008.12.009, 2009.
Thomas, D. N. and Dieckmann, G. S.: Sea Ice – an Introduction to its Physics, Biology, Chemistry and Geology, Blackwell Science, London, 2003.
Thomas, D. N., Papadimitriou, S., and Michel, C.: Biogeochemistry of sea ice, in: Sea Ice, 2nd. Edn., Blackwell Science, London, p. 621 , 2010.
Tison, J. L., Haas, C., Gowing, M. M., Sleewaegen, S., and Bernard, A.: Tank study of physico-chemical controls on gas content and composition during growth of young sea ice, J. Glaciol., 48, 177–191, 2002.
Tison, J. L., Worby, A., Delille, B., Brabant, F., Papadimitriou, S., Thomas, D., de Jong, J., Lannuzel, D., and Haas, C.: Temporal evolution of decaying summer first-year sea ice in the Western Weddell Sea, Antarctica, Deep-Sea Res. Pt. II, 55, 975–987, doi:10.1016/j.dsr2.2007.12.021, 2008.
UNESCO: Eight report of the joint panel on oceanographic tables and standards, Technical papers in Marine Science, 28 pp., 1978.
Untersteiner, N.: Natural desalination and equilibrium salinity profile of perennial sea ice, J. Geophys. Res., 73, 1251–1257, 1968.
Vancoppenolle, M., Goosse, H., de Montety, A., Fichefet, T., Tremblay, B., and Tison, J. L.: Modeling brine and nutrient dynamics in Antarctic sea ice: the case of dissolved silica, J. Geophys. Res.-Oceans, 115, C02005, doi:10.1029/2009jc005369, 2010.
Versteegh, E. A. A., Blicher, M. E., Mortensen, J., Rysgaard, S., Als, T. D., and A. D. Wanamaker Jr.: Oxygen isotope ratios in the shell of *Mytilus edulis*: archives of glacier meltwater in Greenland?, Biogeosciences, 9, 5231–5241, doi:10.5194/bg-9-5231-2012, 2012.

BGD
11, 4047–4083, 2014

Wiesenburg, D. A. and Guinasso Jr., N. L.: Equilibrium solubility of methane, carbon monoxide and hydrogen in water and seawater, J. Chem. Eng. Data, 24, 356–360, 1979.

Yamamoto, S., Alcauskas, J. B., and Crozier, T. E.: Solubility of methane in distilled water and seawater, J. Chem. Eng. Data, 21, 78–80, doi:10.1021/je60068a029, 1976.

Zemmelink, H. J., Delille, B., Tison, J. L., Hintsa, E. J., Houghton, L., and Dacey, J. W. H.: CO_2 deposition over the multi-year ice of the western Weddell Sea, Geophys. Res. Lett., 33, L13606, doi:10.1029/2006GL026320, 2006.

Zhou, J. Y., Delille, B., Eicken, H., Vancoppenolle, M., Brabant, F., Carnat, G., Geilfus, N. X., Papakyriakou, T., Heinesch, B., and Tison, J. L.: Physical and biogeochemical properties in landfast sea ice (Barrow, Alaska): insights on brine and gas dynamics across seasons, J. Geophys. Res.-Oceans, 118, 3172–3189, doi:10.1002/jgrc.20232, 2013.

Zhou, J., Tison, J.-L., Carnat, G., Geilfus, N.-X., and Delille, B.: Physical controls on the storage of methane in landfast sea ice, The Cryosphere Discuss., 8, 121–147, doi:10.5194/tcd-8-121-2014, 2014.

The National Oceanic and Atmospheric Administration (NOAA): Barrow, Alaska, United States (BRW), continous in-situ CATS GC measurements, available at: http://www.esrl.noaa.gov/gmd/obop/brw/index.html, 2013.

BGD
11, 4047–4083, 2014

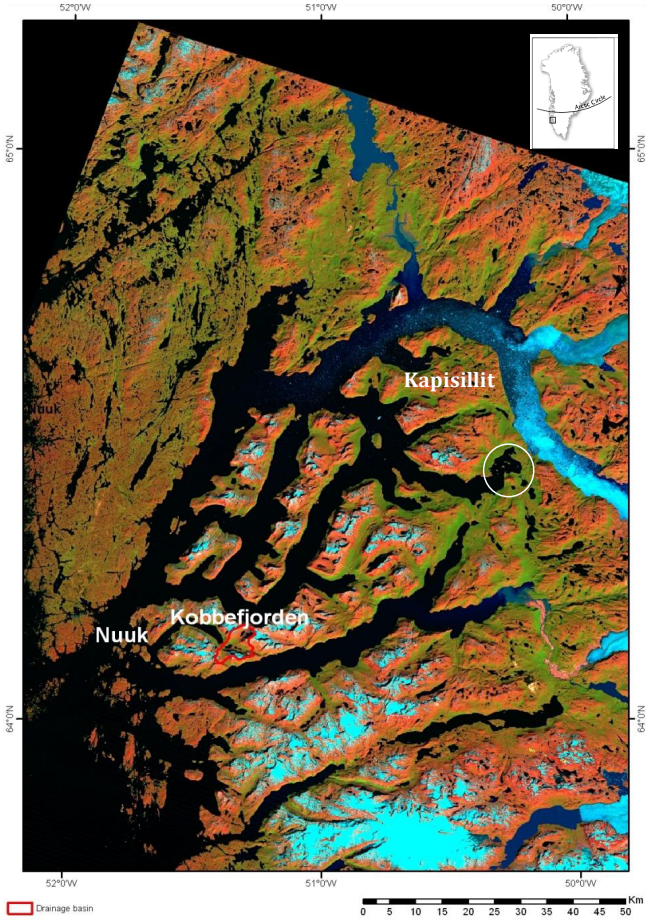

Fig. 1. Study site – landfast sea ice in Godthåbsfjord, SW Greenland. Circle includes the Bay with the study site and the settlement Kapisillit.

BGD
11, 4047–4083, 2014

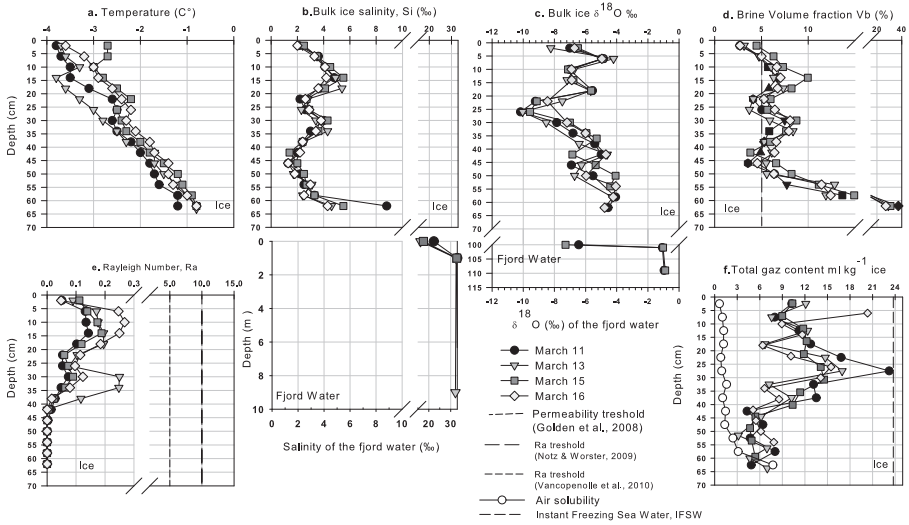

Fig. 2. (a) Bulk ice temperature, **(b)** bulk ice salinity, S_{ice} and underneath water salinity, **(c)** bulk ice $\delta^{18}O$ content and $\delta^{18}O$ of the underneath water, **(d)** brine volume fraction V_b, the dashed line is a reference value for the permeability threshold following Golden et al., 1998, 2007, **(e)** Rayleigh number, *Ra*, the solid and dotted lines are a reference value for the convection threshold according to Notz and Worster (2009) and Vancopenolle et al. (2010), respectively, **(f)** the total gas content in the ice cover, the white circle represent the air concentration at saturation within the ice and the dotted line is a refrence value for the total gas content for Instant Freezing Sea water (Cox and weeks, 1982).

BGD
11, 4047–4083, 2014

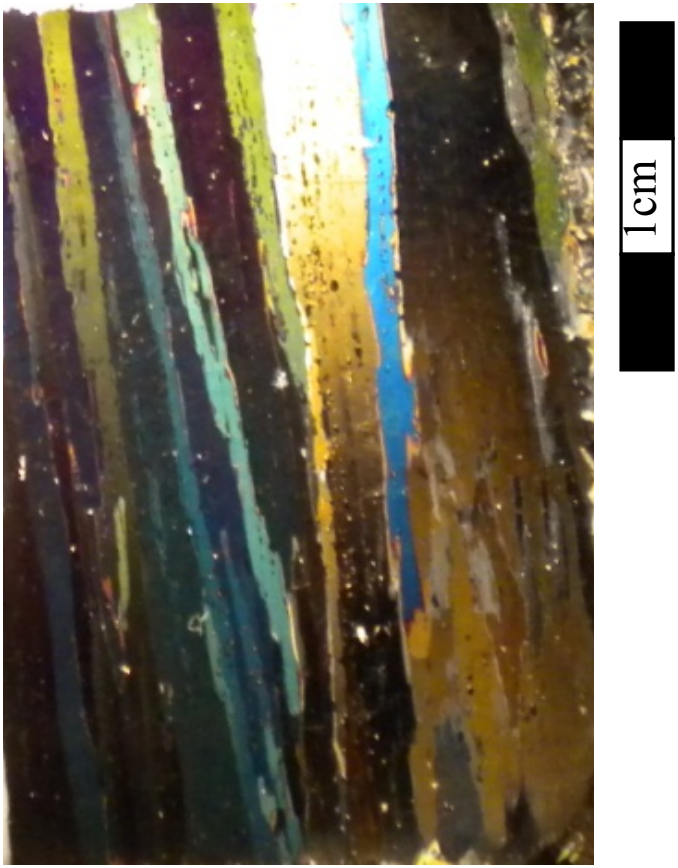

Fig. 3. Tilted columnar ice crystal from 15 March (right) between 24 cm and 32 cm below the sea ice surface.

BGD
11, 4047–4083, 2014

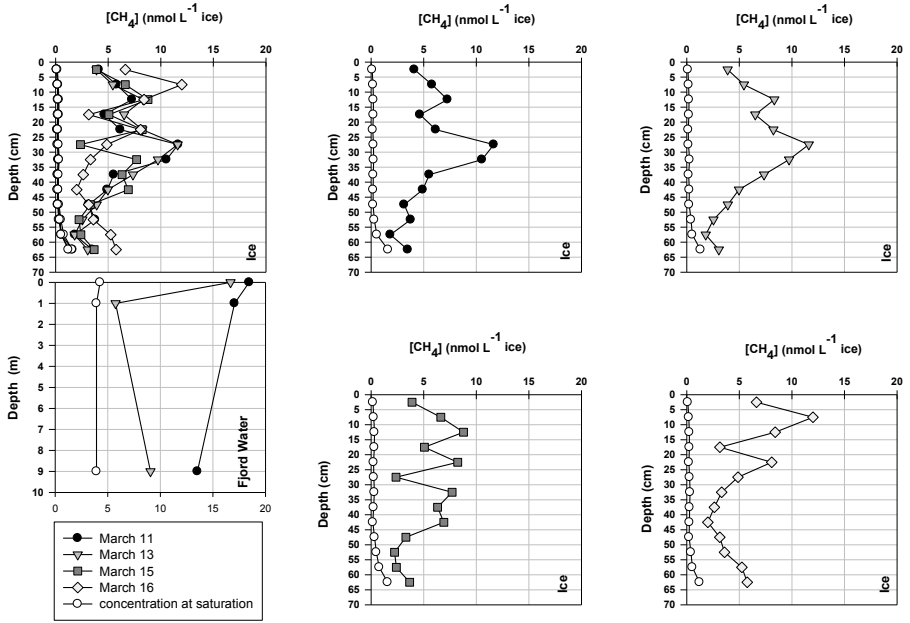

Fig. 4. Evolution of CH_4 concentration ($[CH_4]_{bulk\ ice}$) in bulk sea ice as compared to the concentration at saturation (white circle). The latter was obtained by multiplying the calculated solubility in brine (nmol L^{-1} brine) by the relative brine volume (L brine L^{-1} bulk ice).

BGD
11, 4047–4083, 2014

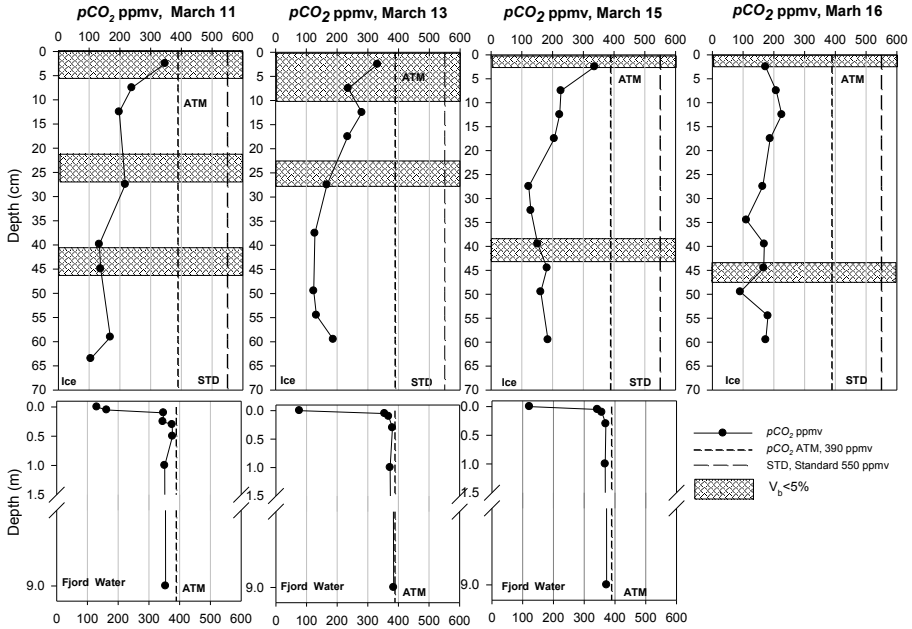

Fig. 5. In the upper part of the figure: high-resolution pCO_2 profiles for each station. The long dashed lines show standard gas concentration used for equilibration (STD, 550 ppmv). The hatched areas show impermeable layer within the ice cover. Ice layers are assumed to be permeable when their brine volume fraction exceeds 5 % (Golden et al., 1998).The lower part of the graph shows the pCO_2 of the fjord water. In each graph the short dotted line shows the atmospheric CO_2 concentration.

BGD
11, 4047–4083, 2014

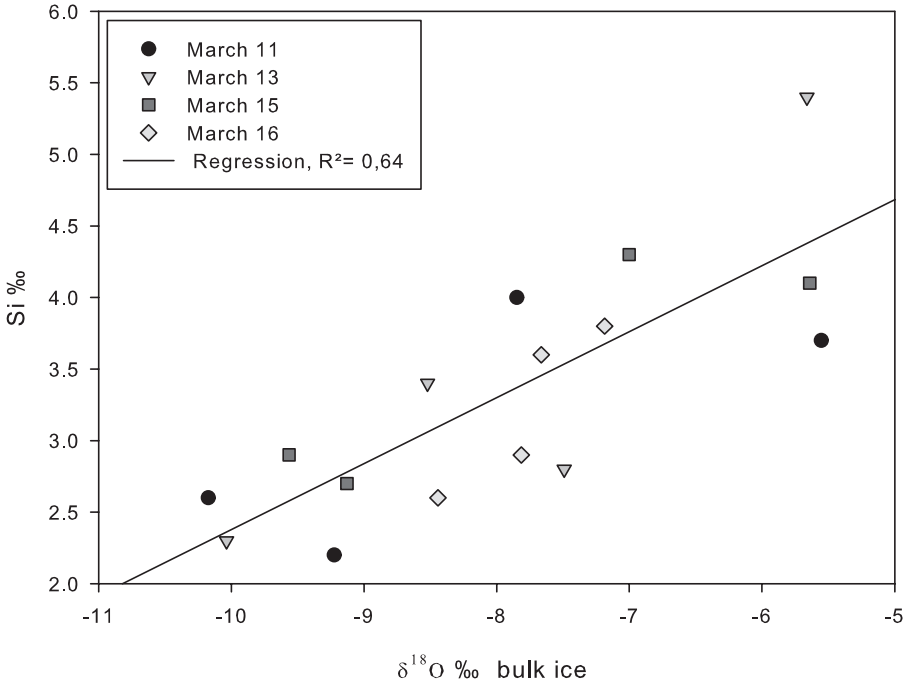

Fig. 6. Relationship between the bulk ice $\delta^{18}O$ content and bulk ice salinity from 20 cm to 30 cm below the ice surface.

BGD
11, 4047–4083, 2014

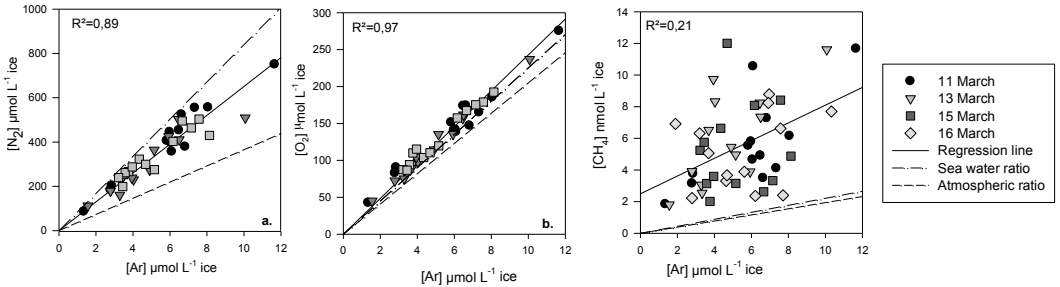

Fig. 7. Relationship between N_2, O_2, CH_4 and Ar concentration within the sea ice cover. The solid line is the regression line. The slope of the dashed equals to the sea water ratio (N_2 : Ar, O_2 : Ar, CH_4 : Ar) while the slope of dotted-dashed line equals to the atmospheric ratio (N_2 : Ar, O_2 : Ar, CH_4 : Ar).

BGD
11, 4047–4083, 2014